Journal Of Materials Chemistry C

Dynamic Article Links ►

Cite this: DOI: 10.1039/c0xx00000x

PAPER

www.rsc.org/xxxxxx

Optically and electrically tunable graphene quantum dot-polyaniline composite films

C. M. Luk[a] , B. L. Chen[a] , K. S. Teng[b], L. B. Tang[a] and S. P. Lau*[a]

Received (in XXX, XXX) Xth XXXXXXXXX 20XX, Accepted Xth XXXXXXXXX 20XX

DOI: 10.1039/b000000x

Graphene quantum dot-polyaniline (PANI-GQD) composite films were synthesized by chemical oxidation polymerization process. The optical properties of the PANI-GQD composite were studied by varying the mole concentration of PANI and the size of the GQDs. The Au/PANI-GQDs/ITO sandwich device was fabricated in order to investigate the transport properties of the composite. A stable hysteresis loop was observed in response to the applied voltage. By varying the PANI content and size of the GQDs, the area within the hysteresis loop and electrical conductance behavior of the device can be tuned in a controlled manner. Both the tunable luminescence and electrical hysteresis behavior are attributed to surface states of the GQDs. The PANI-GQD composite films are expected to find application in photonic devices.

Introduction

Nanocomposite materials with the combination of nanoparticles and polymer have demonstrated superior electrical, optical and mechanical properties [1-8]. The general obstruction to the large-scale production and commercialization of nanocomposites is the lack of cost effective methods for controlling the dispersion of nanoparticles in the polymer matrix. It is because nanoparticles typically aggregate, in turn, it restricts the benefit of size-dependent properties of nanoparticles. The lack of structure-related properties of nanocomposites is another reason for the limited application [3]. Hence, it is of great interest to study various kinds of nanoparticle-polymer composite having different nanoparticles sizes and shapes. Among various conducting polymers, such as p-phenylenevinylene (PPV), polypyrrole (PPy) and polyaniline (PANI), PANI is an unique and promising polymer for practical applications due to its simple preparation, environmental stability, low cost and reversible control of electrical properties by both charge-transfer doping and protonation [9, 10]. Recent studies have demonstrated that incorporation of various nanomaterials into PANI matrix is able to alter the electrical properties and mechanical properties of the polymer matrix. For instance, Zhu *et al.* [11] prepared functional-multiwall carbon nanotubes MWCNT/PANI composite films which were synthesized by electrochemical co-deposition. Berzina *et al.* [12] synthesized gold nanoparticles/PANI composite materials by the polymerization of anilinium, and this resulted in the formation of Schottky barriers between PANI and gold particles.

The bistable electrical conductivity of the composites with one-dimensional nanostructures and organic materials has been reported [13-15]. The mechanisms of electrical bistability and memory effect are dependent on the material system [16-19]. It is worthwhile to investigate the electrical properties of composites that are based on zero-dimensional system. Among the candidates, graphene quantum dots (GQDs) have emerged as one of the most significant zero-dimensional materials because of their fascinating optical [20-27], electronic [28] and spin [29, 30] properties induced by quantum confinement effects and edge effects. To date, a number of techniques have been developed to prepare GQDs, including chemical synthesis [31-35], electrochemical method, graphene oxide reduction [27, 36] and C_{60} catalytic transformation [37]. In fact, GQDs have been considered as an important candidate for applications in photovoltaic [25, 32], bioimaging [26] and light-emitting devices [22, 38].

In this work, we reported a facile, low-cost synthesis in which the PANI-GQD composite can be prepared through a chemical oxidation polymerization process. The luminescence of the GQDs was found to be tunable by varying the content of the PANI. Furthermore, the electrical hysteresis behavior of the composite was observed. The hysteresis effect of the device can be tuned by the concentration and the size of the GQDs.

Experimental methods

The GQDs was prepared by a microwave-assisted hydrothermal method where 3 wt% of glucose powder was dissolved in deionized (DI) water [38, 39]. The as-prepared solution was siphoned to a glass bottle with tightened cover. Then, the glass bottle was irradiated in a microwave oven (CEM Discover SP) at 300 W with a fixed period of 5 minutes. The size of the GQDs can be varied from 3.2 to 11.9 nm as the reaction pressures increased from 165 to 350 psi, respectively.

The reaction temperature was kept constant at 180 ℃. In the process of microwave heating, the solution colour changed from transparent to pale yellow as a result of GQDs formation. The glass bottle was cooled to room temperature under atmosphere condition. In order to prepare the PANI-GQD composite, hydrochloride acid (HCl; 37%) was dispersed in the aniline to form anilinium salt solution by protonation of aniline monomer. The GQD solution was directly added to the salt solution with different mole numbers of aniline. The mixture was heated at 80 ℃ for 30 minutes and then cooled to room temperature. The anilinium ions were attached to the GQDs in the aqueous solution under thermal annealing via charge-charge interactions. The ammonium persulfate (APS) was purified before adding to the mixture. The purification procedure is described as followed: (i) the massive amount of APS powder was dissolved in DI water to reach a saturated solution. (ii) The solution was cooled at 0 ℃ for more than 1 hour. (iii) Re-crystallization of APS was obtained. (iv) The APS crystals were filtered and dried at 50 ℃. Subsequently, the polymerization was taken place at 4 ℃ for 30 minutes. The obtained dark green dispersion was centrifuged at 10000 rpm for 15 minutes. The synthesis process is shown in Figure 1a. For comparison, pure PANI was also synthesized under the same reaction condition. In order to study the electrical characteristics of the composite, 0.5 mL of the solution was drop-casted on the ITO glasses. The ITO glasses were completely covered by the solution. The films were kept at room temperature for 24 hours and then annealed at 75℃ for 2 hours. The patterned gold electrodes with a thickness of 100 nm were fabricated by thermal evaporated deposition.

Transmission electron microscopy (TEM) and high resolution TEM (HRTEM) were performed on JEOL, JEM-2100F at the operating voltage of 200 kV. The morphology and height characterization of the GQDs were carried out by atomic force microscopy (AFM) (Digital Instruments NanoScope IV) operating in tapping mode. The Fourier transform infrared (FT-IR) spectra of the samples were obtained using KBr pellet method by Nicolet Magna-IR 760 spectrometer with a resolution of 4 cm^{-1}. The UV-Vis spectra were carried out on a Shimadzu UV-2550 UV-Vis spectrophotometer at room temperature. Photoluminescence (PL) measurements on the samples were performed using FLS920P Edinburgh Analytical Instrument apparatus. Xe lamp was used as an excitation source. The current-voltage measurements were carried out using probes station with a programmable electrometer Keithley (model 2400). The X-ray photoelectron spectroscopy (XPS) experiment was performed using Al Kα source with energy of 1486.6 eV at room temperature (VG ESCAlab MKII).

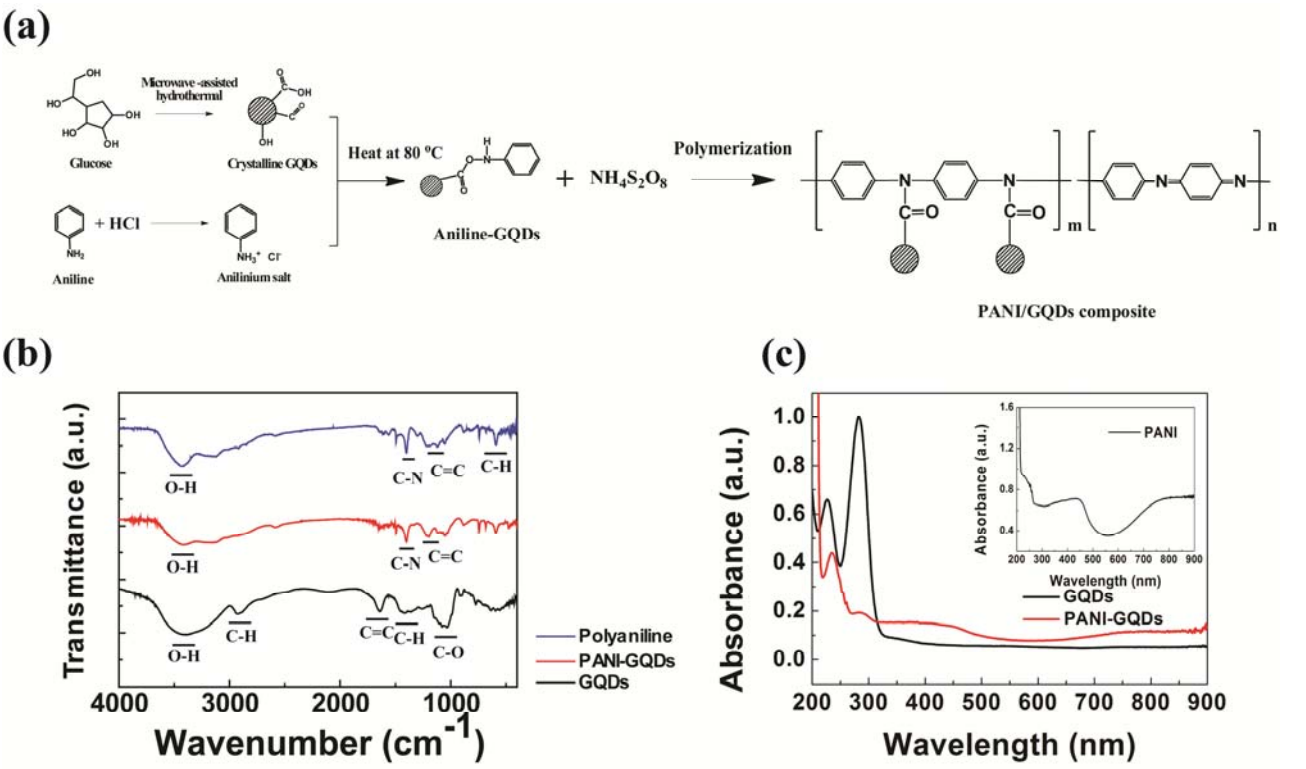

Figure 1(a) Schematic diagram for the preparation of the PANI-GQD composite. (b) FT-IR spectra of the PANI, PANI-GQDs and GQDs. The GQDs was fabricated under the reaction pressure of 165 psi. (c) UV-Vis absorbance of the GQDs, and PANI-GQDs. The inset shows the absorbance of pure PANI.

Results and discussion

The functional groups of the GQDs were identified using FT-IR spectroscopy, as shown in Figure 1b. The spectrum of the GQDs exhibits a C=C stretching at 1641 cm^{-1}, which is an elementary unit of the GQD core. An O-H stretching can be observed at the peak of 3392 cm^{-1}. The existence of C-O in the GQD is confirmed by the presence of absorption bands at 1026 and 1076 cm^{-1}. The absorption bands at 1415 and 2929 cm^{-1} are resulted from the C-H bonding. With regard to PANI, peaks at 1490 cm^{-1} and 1396 cm^{-1} are ascribed to the stretching vibration of benzenoid ring and C-N of the aromatic secondary amines. The peak at 1139 cm^{-1} is attributed to the in-plane bending vibrations of the benzene ring. In the spectrum of PANI-GQDs, almost all the FT-IR peaks of the PANI are maintained. However, these peaks shifted to higher frequencies at 1502 cm^{-1} (benzenoid ring), 1402 cm^{-1} (C-N of the secondary amines) and 1199 cm^{-1} (in-plane benzene ring) respectively. This might be explained by the conjugation between the GQDs and PANI. In addition, the peak at 1052 cm^{-1} (the C-O characteristics peak of GQDs) appears in the spectrum of PANI-GQD, which suggests that the oxygenated functional groups on the GQDs play an important role in the formation of the composites.

Complementary to the FT-IR results, the UV-Vis absorption spectra of the GQDs and composites are shown in Figure 1 (c). Two strong UV absorption peaks at 228 and 284 nm are found in the GQD spectrum. The absorption peaks at 228 and 284 nm are similar to that of the GQDs prepared by hydrothermal graphene oxide GO reduction method (230 and 320 nm) [20]. The peak at 228 nm is caused by π to π^* transition of C=C, while the peak at 284 nm is attributed by n to π^* transition of the C=O bond [40]. The PANI-GQD composite shows mainly four characteristic peaks at 236, 284, 420 and 850 nm. The first two peaks (236 and 284 nm) were derived from the GQDs. The shift of the peak from 228 to 236 nm of GQDs might be attributed to the conjugation between the GQDs and PANI [41]. The other peaks at 420 and 850 nm were attributed to the polarization zone transition of PANI [42]. Furthermore, the ratio of the peak of C=O to that of C=C transition in the composite became smaller in comparison of the GQDs. The above results showed that the GQDs and PANI conjugate existed in the PANI-GQD composite.

We performed XPS on the samples to determine the surface composition and bonding of the PANI-GQD, as shown in Figure 2. The survey XPS of the composite is mainly dominated by the signals of C, O and N. For the parent GQDs, the measured C1s spectrum can be fitted with five components, such as 284.5 eV (sp^2 bonded carbon), 285.3 eV (sp^3 bonded carbon), 286.5 eV (C-OH group), 287.1 eV (C-O-C group) and 288.1 eV (C=O group). The surface components of the GQDs obtained using XPS are consistent with the FT-IR results. Similar components were also observed at the measured C1s spectrum of PANI-GQD. For N1s spectrum of the composite, the curve can be deconvoluted into three components, which are 399.5 eV (pyridinic N), 401.0 eV (pyrrolic N) and 402.1 eV (graphitic N). The C/O and C/N atomic ratio for the PANI-GQD is 2.31 and 7.75 respectively.

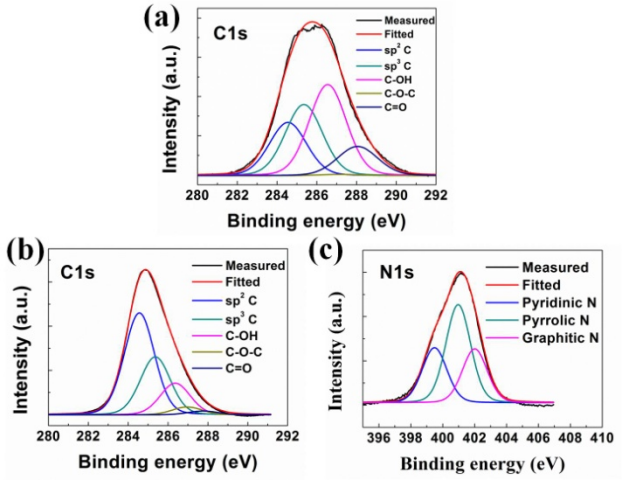

Figure 2 C1s XPS spectrum of (a) the GQDs, (b) PANI-GQD. (c) N1s spectrum of the PANI-GQD.

Figure 3 shows the typical TEM images of the GQDs and PANI-GQD dispersed on the copper grid. The images revealed highly monodispersed property of the GQDs, which is one of the major advantages of our GQDs preparation method [39]. The presence of lattice fringe of 0.247 nm, which corresponds to the basal plane distance of bulk graphite [39], is shown in the inset of Figure 3a. The average size of the GQDs is 3.42 ± 0.15 nm when the reaction pressure is 165 psi. As the reaction pressure increased to 350 psi, the size of the GQDs increased from 3.4 to 11.9 nm. The TEM images of the GQDs prepared at different reaction pressures are shown in Figure S1 in ESI†. At first glance, glucose molecules undergo carbonizing, nucleating, crystallizing and growing up. Since the core of the GQD is composed of C=C bonding, the functional groups can only exist at the surface of the GQD, as confirmed by FT-IR and XPS spectra. Hence the growth occurs only at the interface of the GQD. Because of the high pressure induced by the hydrothermal condition, the C=C bonding is arranged in an orderly manner and assist in the growth of crystalline GQD. As the pressure increases, the growth rate of the GQD becomes faster. The existence of the hydrophilic functional groups such as –OH, C-O-R and –C=O on the surface makes the GQDs water soluble.

The surface morphology of the GQDs dispersed on the SiO_2/Si substrate was studied by atomic force microscopy (AFM). Figure 3c shows three randomly selected GQDs labeled as A, B and C. The average height of these GQDs is about 3.2 nm, corresponding to a few atomic layers (~ 5 layers) GQDs. Figures 3e and 3f show the TEM images of the GQDs embedded in PANI. The results depict an almost uniform distribution of GQDs in the polymer matrix. Furthermore, the shape of the GQDs in the composite become irregular compared with the as-prepared GQDs, probably owing to the surface modification of the GQDs from chemical reaction between the functional groups located at the GQDs surface and polymer matrix.

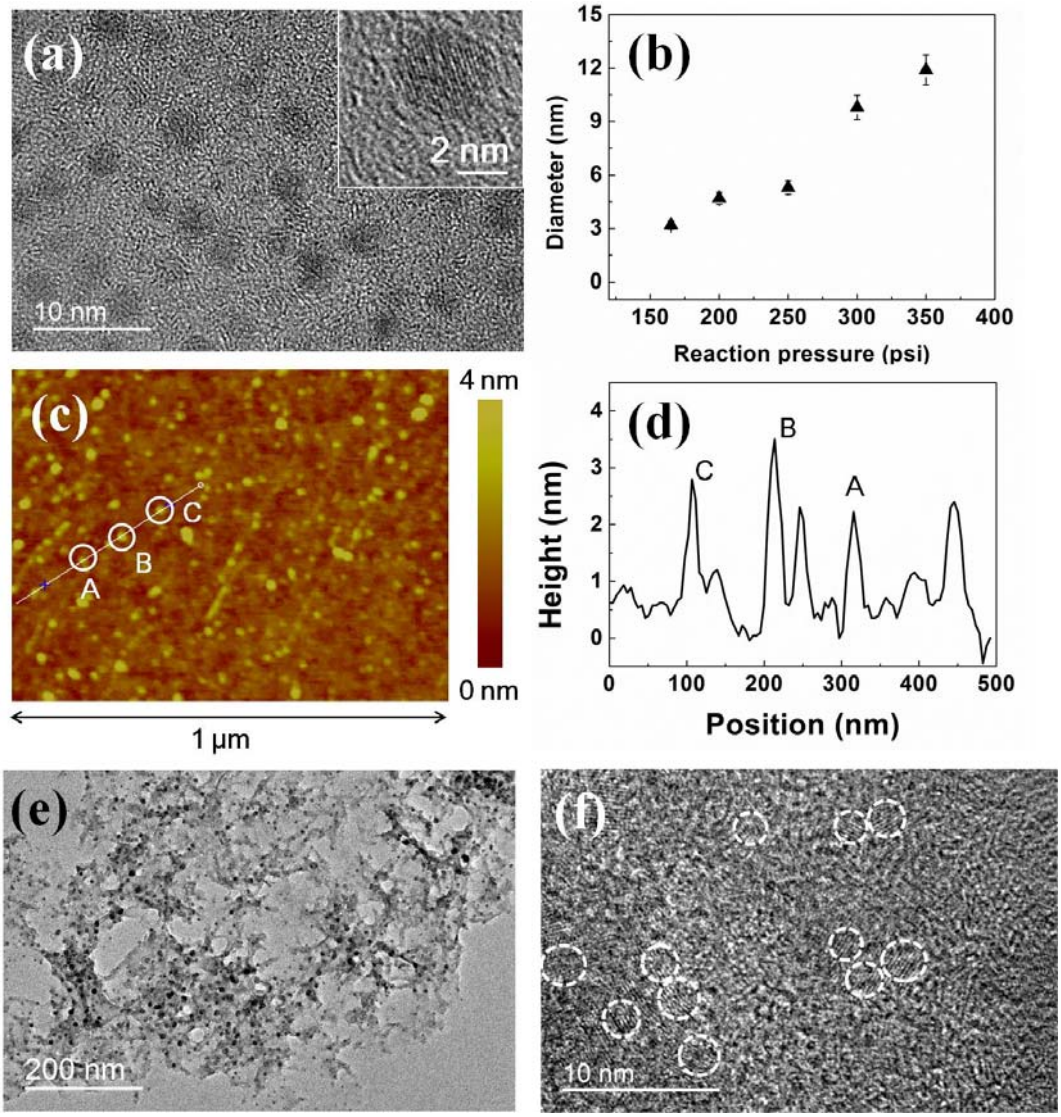

Figure 3 (a) High-resolution TEM image of the GQDs. (b) The diameter of the GQDs for various reaction pressures. (c) AFM image of the GQDs. (d) The height analyses of the GQDs as shown in AFM image (c). (e) and (f) low magnification and High-resolution TEM images of the PANI-GQD composite respectively.

The photoluminescence (PL) spectra of the GQDs and PANI-GQD composites are shown in Figure 4. The excitation wavelength is 365 nm. For the GQDs with the diameter of 3.2 nm, the PL peak position of the GQDs is 454 nm. The PL emission peak is shifted to 489 nm after the functionalization of polyaniline with a mole number of 1 mmol. Since the size of the as-received GQDs and GQDs in PANI are similar; the redshift behavior is primarily attributed to aniline functionalization. We hypothesize that the aniline functional groups (amine group, -NH) can contribute to the electron donation from the amine group to the GQDs based on induced electron withdrawal, making π-conjugated system more electrophilic [43]. In the view of organic chemistry, since the GQD has large π-conjugated system, the electron donating group can be excited to the aromatic rings to form p-π conjugated system, thus enlarging the π-conjugated system [43]. The strong orbital interaction between aniline and π-conjugated system elevates the primary HOMO to a higher energy orbit [44]. To support this hypothesize, we varied the concentration of PANI to observe the PL shifts of the composites. The emission wavelength is shifted from 489 to 515 nm when the mole number increases from 1 to 5 mmol. The increased amount of amine group would enhance electron delocalization densities, resulting in a much narrower optical band gap. The emission of the GQDs can also be tuned by changing the size of the GQDs (Figure S2 in ESI†). It is clearly seen that the PL emission is shifted from 456 to 598 nm with increasing GQD size, which demonstrated similar trend observed in other quantum dots due to quantum confinement effect [45]. The observed different emission from the different-sized GQDs is the result of variation in the nature of sp^2 bonding and density available at the GQDs [46]. Since the GQDs were shown to exhibit excitation dependent PL emission in some previous works [38, 39], a detailed PL measurement for the PANI-GQD composite was performed at different excitation wavelengths, as shown in Figure S3 in ESI†. The excitation wavelength was

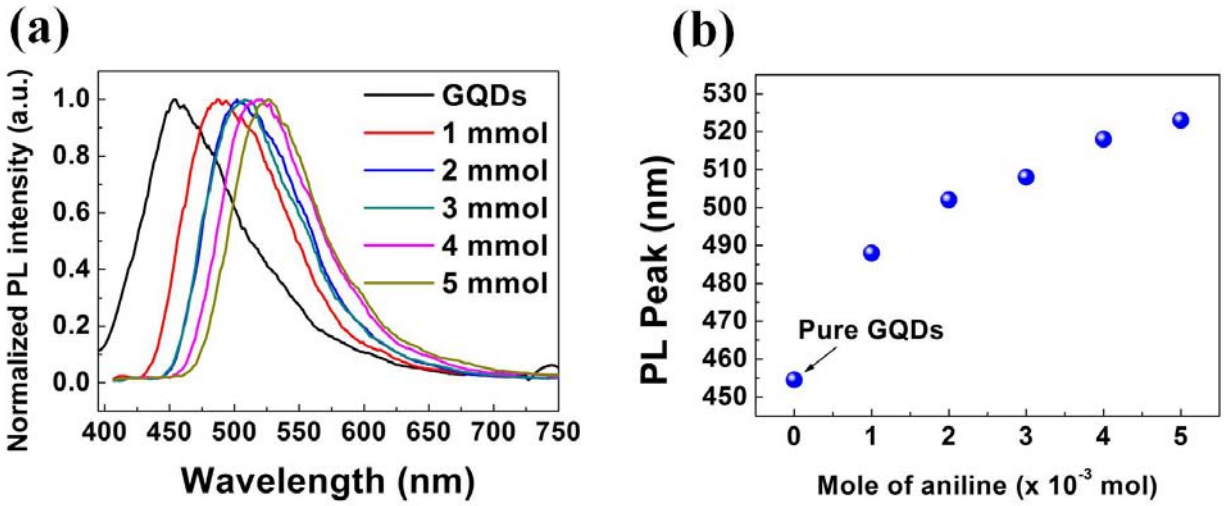

Figure 4. (a) Photoluminescence (PL) spectra of the PANI-GQDs with various moles of aniline. (b) The dependence of the PL emission on mole number of aniline.

adjusted from 330 nm to 470 nm. Figure S3 (g) shows the overall summary of the PL emission of the composites with various excitation wavelengths. For the parent GQDs, The PL shifts from 440 nm to 554 nm when the excitation wavelength changed from 330 nm to 470 nm. With regard to the mole number of PANI, all the composites also show excitation-dependent emission which has a similar trend with the GQDs. The phenomenon of the excitation dependent emission in the GQDs and PANI-GQDs could be related to the surface states located at the GQD surface which will be discussed later.

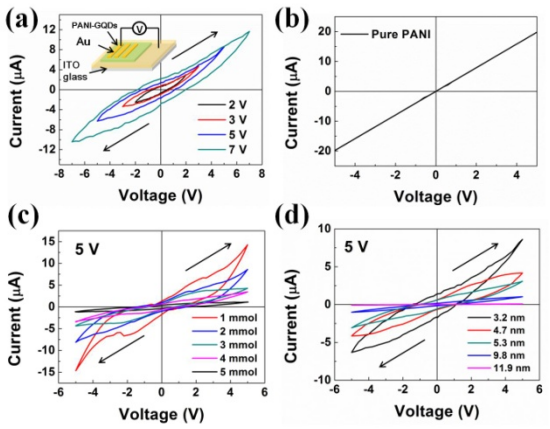

Figure 5 (a) Hysteresis behavior of the Au/PANI-GQD/ITO structure under different voltages. The inset depicts the device structure. (b) Linear relationship of the current-voltage characteristics of PANI. Hysteresis loops measured at (c) various moles of aniline and (d) sizes of the GQDs respectively. All the hysteresis behaviors were measured in clockwise direction with respect to the voltage.

The Au/PANI-GQDs/ITO sandwich-structure device was prepared in order to study the electrical transport properties of the composite. The schematic diagram of the device is shown in the inset of Figure 5a. A nonlinear response of the PANI-GQD composite with significant hysteresis was observed, while the pure PANI exhibits a linear current-voltage relationship as shown in Figure 5a and 5b, respectively. From the results shown, the electrical hysteresis behavior is reproducible by varying the maximum sweeping voltage, but independent on the sweep direction (either in clockwise or anti-clockwise direction). The formation of the hysteresis loop in both positive and negative bias voltage shows a characteristic memory phenomenon.

The I-V characteristics of the composites varied with the concentration of the PANI contained in the composite is shown in Figure 5c. The hysteresis with large amount of PANI is less pronounced. We also studied the effects of the size of the GQDs on the electrical characteristics in the composites (Figure 5d). It is noted that the increase of the GQD size would lead to a decrease in the conductivity, and the hysteresis loop would also become smaller. The presence of the GQDs with various sizes may modulate the conduction paths. The area within the hysteresis loop as a function of applied bias voltage, diameter of GQDs and content of PANI are depicted in Figures 6a and 6b. The area within the hysteresis loop is equivalent to the energy stored in the composite film. The hysteresis loop enlarged with increasing bias voltage amplitude, which can be explained by voltage induced conformational changes in the polymer structure [47] resulted from stronger detrapping and spartial distribution of charges at higher voltage amplitude.

As demonstrated above, our GQDs consists of C=C core, O and H related functional groups at the surface. These functional

groups, including C-OH, C-H, C-O, at the surface form "surface states" located at the energy level between π and π* states of C=C. The surface states energy level can be estimated by the energy difference between the intrinsic absorption energy at 228 nm (5.44 eV) and the surface state absorption energy at 282 nm (4.40 eV). Thus, the surface states level is located at ~ 1.0 eV above π energy level of the GQDs [39]. The functional groups have various energy levels, therefore resulting in different emissive traps. When a certain excitation wavelength illuminates the GQDs, the emission is dominated by the surface state emission trap. However, the intrinsic absorption for PANI-GQD composites is shifted to 236 nm (5.25 eV) and this changes the location of the surface states, which become ~ 0.85 eV above π energy level (Figure 6c). This makes easier for the charges to tunnel via the surface states. Hence, the surface states in the composite serves not only as various emission traps, but also as 'charge trapping centers'. Variations in surface states are expected as the electron delocalization densities changes as a result of changing PANI concentration. Consequently, it results in the change of the hysteresis behavior. The surface states induced by the functional groups plays an important role in both the tunable emission and hysteresis conducting behaviors of the PANI-GQDs composite.

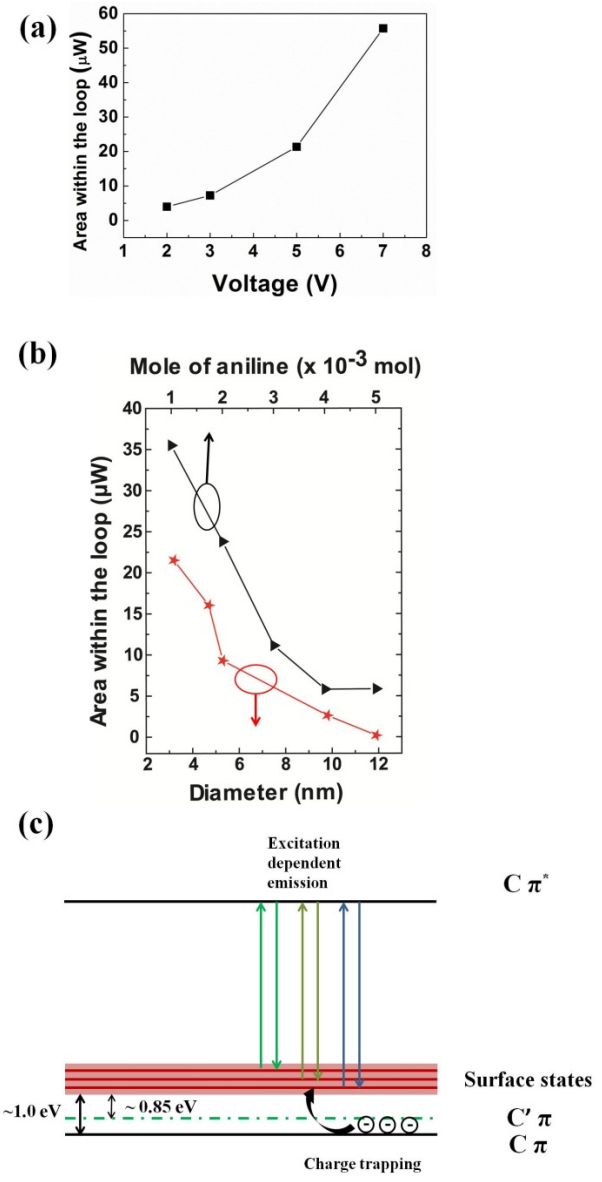

Figure 6 Plot of the area within the hysteresis loops as a function of (a) biased voltage, (b) mole number of aniline and diameter of the GQDs. (c) Schematic diagram of the energy level of the GQDs. The dash line (C'π) indicates the new intrinsic absorption of the PANI-GQD.

Conclusions

In conclusion, we have demonstrated the tunable PL and hysteresis behavior for GQDs embedded in PANI matrix. The PL redshift in the composite is attributed to π-conjugated system interaction between GQDs and PANI. The electrical measurements show a stable clockwise hysteresis loops under both forward and reverse bias in I-V characteristics. The conductivity and hysteresis behavior can be tuned by changing the amounts of PANI and sizes of the GQDs. The controllable electrical and optical properties in the composite films are explained by the charge trapping sites located at the surface states induced by the functional groups. This work may open a wide range of application for GQD composite based devices.

Acknowledgements

This work was financially supported by the Research Grants Council of Hong Kong (Project No. PolyU 5006/12P), PolyU grants (Project Nos. G-YJ70, G-YN10 and 1-ZV8N) and National Natural Science Foundation of China (Grant no. 11374250)

Notes and references

[a] *Department of Applied Physics, The Hong Kong Polytechnic University, Hung Hom, Kowloon, HKSAR and The Hong Kong Polytechnic University Shenzhen Research Institute, Shenzhen 518057, China; E-mail: apsplau@polyu.edu.hk*

[b] *Multidisciplinary Nanotechnology Centre, College of Engineering, Swansea University, Singleton Park, Swansea SA2 8PP, UK*

† Electronic Supplementary Information (ESI) available: [TEM images, size distribution of the GQDs, PL spectra of the GQDs with different sizes and excitation dependent PL spectra with different mole of aniline]. See DOI: 10.1039/b000000x/

1. L. Ye, L. Z. Lai and J. Liu, IEEE Trans. Electron. Packag. Manuf., 1999, 22, 299.
2. Y. Song, Y. Shen, H. Liu, Y. Lin, M. Li and C. W. Nan, J. Mater. Chem., 2012, 22, 8063.
3. A. C. Balazs, T. Emrick and T. P. Russell, Science, 2006, 314, 1107.
4. A. Haryono and W. H. Binder, Small, 2006, 2, 600.
5. W. T. Kim, J. H. Jung, T. D. Kim and D.I. Son, Appl. Phys. Lett., 2010, 96, 253301.
6. M. S. Mehata, M. Majumder, B. Mallik and N. Ohta, J. Phys. Chem. C, 2010, 114, 15594.
7. M. Majumder, A. K. Chakraborty, B. Biswas, A. Chowdhury and B. Mallik, Synth. Met., 2011, 161, 1390.
8. D. I. Son, D. H. Park, J. B. Kim, J. W. Choi, T. W. Kim, B. Angadi, Y. Yi and W. K. Choi, J. Phys. Chem. C, 2011, 115, 2341.

9. A. A. Syed and M. K. Dinesan, Talanta, 1991, 38, 815 – 837.
10. A.G. MacDiarmid, Rev. Mod. Phys. 2001, 73, 701.
11. Z. Z. Zhu, Z. Wang, H.L. Li, Appl. Surf. Sci., 2008, 254, 2934.
12. T. Berzina, A. Pucci, G. Ruggeri, V. Erokhin and M. P. Fontana, Syn. Met. 2011, 161, 1408.
13. B. Biswas, A. Chowdhury, B. Mallik, RSC Adv. 2013, 3, 3325.
14. A. Sleiman, M. F. Mabrook, R. R. Nejm, A. Aayesh, A. A. Ghaferi, M. C. Petty, D. A. Zeze, J. Appl. Phys., 2012, 112, 024509.
15. M. Rinkio, M. Y. Zavodchikova, P. Torma, A. Johansson, Phys. Status Solidi B, 2008, 245, 2315.
16. C. Li, G. Hai-Ming, Z. Xi, D. Shi-Xuan, S. Dong-Xia, G. Hong-Jun, Chin. Phys. B, 2009, 18, 1622.
17. S. L. Lim, N. J. Li, J. M. Lu, Q. D. Ling, C. X. Zhu, E. T. Kang, K. G. Neoh, ACS Appl. Mater. Interfaces, 2009, 1, 60.
18. B. Biswas, A. K. Chakraborty, M. Majumder, A. Chowdhury. M. K. Sanyal, B. Mallik, Synth. Mat., 2012, 161, 2632.
19. Q. D. Ling, S. L. Lim, Y. Song, C. X. Zhu, D. Siu-Hhung Chan, E. T. Kang, K. G. Neoh, Langmuir, 2007, 23, 312.
20. D. Pan, J. Zhang, Z. Li, M. Wu, Adv. Mater. 2010, 22, 734.
21. Z. Z. Zhang, K. Chang, Phys. Rev. B 2008, 77, 235411.
22. V. Gupta, N. Chaudhary, R. Srivastava, G. D. Sharma, R. Bhardwaj, S. Chand, J. Am. Chem. Soc. 2011, 133, 9960.
23. M. L. Mueller, X. Yan, J. A. McGuire, L.-s. Li, Nano Lett. 2010, 10, 2679.
24. R. Liu, D. Wu, X. Feng, K. Müllen, J. Am. Chem. Soc. 2011, 133, 15221.
25. Y. Li, Y. Hu, Y. Zhao, G. Shi, L. Deng, Y. Hou, L. Qu, Adv. Mater. 2011, 23, 776.
26. S. Zhu, J. Zhang, C. Qiao, S. Tang, Y. Li, W. Yuan, B. Li, L. Tian, F. Liu, R. Hu, H. Gao, H. Wei, H. Zhang, H. Sun, B. Yang, Chem. Commun. 2011, 47, 6858.
27. J. Shen, Y. Zhu, C. Chen, X. Yang, C. Li, Chem. Commun. 2011, 47, 2580.
28. K. A. Ritter, J. W. Lyding, Nat. Mater. 2009, 8, 235.
29. J. Güttinger, T. Frey, C. Stampfer, T. Ihn, K. Ensslin, Phys. Rev. Lett. 2010, 105, 116801.
30. B. Trauzettel, D. V. Bulaev, D. Loss, G. Burkard, Nat. Phys. 2007, 3, 192.
31. X. Yan, B. Li, X. Cui, Q. Wei, K. Tajima, L.-s. Li, J. Phys. Chem. Lett. 2011, 2, 1119.
32. X. Yan, X. Cui, B. Li, L.-s. Li, Nano Lett. 2010, 10, 1869.
33. X. Yan, X. Cui, L. Li, J. Am. Chem. Soc. 2010, 132, 5944.
34. L. Li, X. Yan, J. Phys. Chem. Lett. 2010, 1, 2572.
35. M. L. Mueller, X. Yan, B. Dragnea, L.-s. Li, Nano Lett. 2011, 11, 56.
36. J. Shen, Y. Zhu, X. Yang, J. Zong, J. Zhang and C. Li, New J. Chem. 2012, 36, 97.
37. J. Lu, P. S. E. Yeo, C. K. Gan, P. Wu, K. P. Loh, Nat. Nanotechnol. 2011, 6, 247.
38. C. M. Luk, L. B. Tang, W. F. Zhang, S. F. Yu, K. S. Teng, S. P. Lau, J. Mater. Chem., 2012, 22, 22378.
39. L. B. Tang, R. B. Ji, X. K. Cao, J. Y. Lin, H. X. Jiang, X. M. Li, K. S. Teng, C. M. Luk, S.J. Zeng, J. H. Hao, S. P. Lau, ACS Nano, 2012, 6, 5120.
40. Z. Luo, Y. Lu, L. A. Somers, A. T. C. Johnson, J. Am. Chem. Soc., 2009, 131, 898.
41. Y. Mao, Y. Bao, L. Yan, G. Li, F. H. Li, D. X. Han, X. B. Zhang, L. Niu, RSC Adv., 2013, 3, 5475.
42. A. Ray, A. F. Richter, A. G. MacDiarmid, A. J. Epstein, Synth. Met., 1989, 29, 151.
43. R. T. Morrison, R. N. Boyd, Electrophilic Aromatic Substitution in Organic Chemistry, 6th ed., Prentice Hall International, Inc., Upper Saddle River, NJ, 1992, pp. 517-546.
44. S. H. Jin, D. H. Kim, G. H. Jun, S. H. Hong, S. K. Jeon, ACS Nano, 2013, 7 (2), 1239.
45. D. V. Melnikov, J. R. Chelikowsky, Phys. Rev. Lett. 2004, 92. 046802.
46. J. Peng, W. Gao, B. K. Gupta, Z. Liu, R. Romero-Aburto, L. Ge, L. Song, L. B. Alemany, X. Zhan, G. Gao, S. A. Vithayathil, B. A. Kaipparettu, A. A. Marti, T. Hayashi, J.-J. Zhu, P. M. Ajayan, Nano Lett. 2012,12 (2), 844-849.
47. B. Biswas, A. K. Chahraborty, M. Majumder, A. Chowdhury, M. K. Sanyal, B. Mallik, Synth. Mat. 2012, 161, 2632.